**SERBIAN JOURNAL OF ELECTRICAL ENGINEERING**
**Vol. 12, No. 3, October 2015, 359–373**

**UDC: 519.87:537.852]:621.313.323** **DOI: 10.2298/SJEE1503359G**

# A Nonlinear Equivalent Circuit Model for Flux Density Calculation of a Permanent Magnet Linear Synchronous Motor

**Reza Ghanaee[1], Ahmad Darabi[2], Arash Kiyoumarsi[1], Mohammad Reza Baghayipour[2], Mohammad Javad Morshed[1]**

**Abstract:** In this paper, a nonlinear magnetic equivalent circuit is presented as an analytical solution method for modeling of a permanent magnet linear synchronous motor (PMLSM). The accuracy of the proposed model is verified via comparing its simulation results with those obtained by two other methods. These two are the Maxwell's Equations based analytical method and the well-known finite elements method (FEM). Saturation and any saliency e.g. slotting effects can be considered properly by both nonlinear magnetic equivalent circuit and FEM, where it cannot be taken into account easily by the Maxwell's Equations based analytical approach. Accordingly, as the simulation results presented in this paper confirm, the proposed nonlinear magnetic equivalent circuit is compatible with FEM regarding the accuracy while it requires very shorter execution time. Therefore, the magnetic equivalent circuit model of the present paper can be considered as a preferable substitute for the time consuming FEM and approximated analytical method built on Maxwell's Equations in particular when required to be applied for a design optimization problem.

**Keywords:** Finite Elements Method, Flux Density, Maxwell's Equations, Nonlinear Magnetic Equivalent Circuit, Permanent Magnet Linear Synchronous Motor.

## 1 Introduction

In the conventional mechanisms, the linear displacement is produced via using rotating motor and some mechanical interfaces. Linear electrical motors are known as appropriate substitutes for the conventional mechanisms. This is because, in the linear motors, the linear force and displacement are generated directly by the electromagnetic field, without any mechanical interface. Among different linear motors, PMLSMs naturally have great thrust, low losses, small electric time constant and fast response, due to their capability of saving a large

[1]Department of Electrical Engineering, Faculty of Engineering, University of Isfahan, Isfahan, Iran;
E-mails: rghanaee@gmail.com; kiyoumarsi@eng.ui.ac.ir; mj.morshed@gmail.com
[2]Faculty of Electrical Engineering, University of Shahrood, Shahrood, Iran;
E-mails: darabi_ahmad@hotmail.com; mbpower@gmail.com

amount of energy in the permanent magnet. Therefore, PMLSMs are already researched more than the other types of linear motors [1 – 4]. However, one of their drawbacks is the presence of low frequency harmonics, which is because the flux density waveform of the permanent magnet is not an ideal sinusoidal signal. Such harmonics lead to unwanted beats in the thrust and then reduce the accuracy of PMLSMs [5, 6]. In this paper, an accurate and fast model is proposed to calculate the flux density distribution in the air-gap. Not only the proposed model is efficient to calculate the thrust waveform and pulsations accurately, but also it can be used in machine design by intelligent optimization algorithms. Accurate calculation of flux density distribution in the air-gap is an important issues of electrical machine designers. In [7], the air gap flux density has been calculated by the Maxwell's equations, as well the slotting effects have been taken into for machine design. In addition, similar calculation has been studied in [8], without considering the slotting effects. The numerical solution for the nonlinear equivalent magnetic circuit has been done in [9]. An equivalent magnetic circuit was applied to calculate the flux density distribution in air-gap [10]. The main goal of this paper is to propose an accurate analytical model, yet with low computational complexity, for being used in iterative optimization algorithms. Because the Maxwell's equations provide closed formulas for the calculation of motor parameters, and are suitable for iterative optimization techniques. However, disregarding the effects of saturation in the core is the main drawback of this method, so the harmonics of flux density cannot be measured accurately. As well, due to the time consuming calculations involved in FEM, it is not recommended to use in the iterative optimization approaches [10, 11]. On the other hand, the nonlinear magnetic equivalent circuit can be used to machine design studies. Considering effects of core saturation is one of the most important advantages of the nonlinear magnetic equivalent circuit. Anyway, it cannot provide closed formulations for different parameters in motor. As a result, it requires more computation time due to the increase of elements number.

Regarding the fact that the nonlinear magnetic equivalent circuit is indeed a smaller sample of FEM, this paper aims to propose a model based on the nonlinear magnetic equivalent circuit, but having acceptable accuracy as well as appropriate speed. Thus, this model can be used instead of the previous FEM and Maxwell's equations methods which are utilized in the intelligent machine-optimization algorithms. The rest of the paper is organized as follows: in the Section 2, the air-gap flux density distribution is calculated using the Maxwell's equations. In the Section 3, a nonlinear magnetic equivalent circuit with 53 elements is presented. The simulation results of the analytical methods are presented, and are compared to the FEM simulation results in the Section 4. Finally, concludes the paper.

## 2 Analytical Simulation Using Maxwell's Equations

Linear motors are composed of three parts: primary, air-gap, and secondary. The part on which the windings are placed is called "Primary". The moving part (secondary) is classified into two types: Moving magnet, and Moving windings. The permanent magnet linear synchronous motor under analysis is depicted in Fig. 1. The motor comprises one primary and one secondary. The primary is the moving part of motor whose slots have the primary three-phase windings. The secondary is constructed from ferromagnetic materials on which the permanent magnets are consecutively stationed. The motor dimensionality and characteristics are scheduled in **Table 1**.

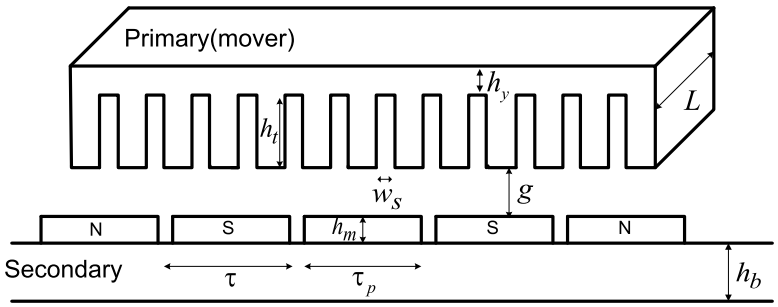


**Fig. 1** – *The topology of the permanent magnet linear synchronous motor.*

**Table 1**
*The motor characteristics.*

| Parameter | Symbol | Unit | Value |
|---|---|---|---|
| Motor width | L | mm | 100 |
| Pole pitch | $\tau$ | mm | 46.5 |
| PM height | $h_m$ | mm | 5 |
| PM width | $\tau_p$ | mm | 40 |
| Relative permeability of PM | $\mu_r$ | - | 1.05 |
| Residual Flux density | $B_r$ | T | 1.2 |
| Slot width | $w_s$ | mm | 6 |
| Slot height | $h_t$ | mm | 15 |
| Slot pitch | $s$ | mm | 15.5 |
| Yoke height | $h_y$ | mm | 10 |
| air-gap length | $g$ | mm | 0.5 |

### 2.1 Magnetic field distribution due to the magnets

Fig. 2 illustrates the layered model of machine supposing that the primary is not excited. The model includes two iron layers are extended along the x-axis direction, permanent magnet layer, and air. In order to calculate the magnetic field distribution, the following suppositions are assumed [12].

1. The stator length along *x*–direction is infinite.
2. The terminative effects along *z*–direction are ignored.
3. The permeability of the permanent magnet is assumed equal to that of vacuum ( $\mu_0$ ).
4. The permeability of the stator yoke is infinite.

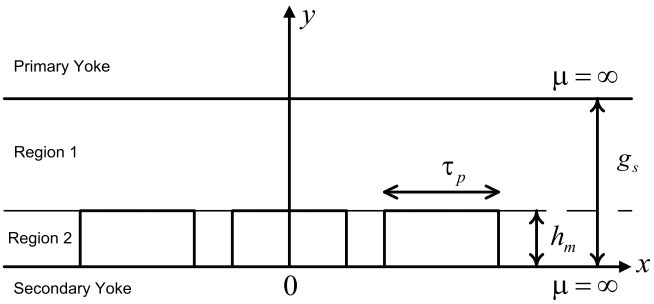


**Fig. 2** – *Definition of the two areas in the machine model.*

In this step, the slotting effects are disregarded. To calculate the magnetic field distribution, Maxwell's Equations are defined with respect to the magnetic vector potential as Laplace and Poisson partial differential equations [8].

$$\begin{cases} \dfrac{\partial^2 A_1}{\partial x^2} + \dfrac{\partial^2 A_1}{\partial y^2} = 0 \\ \dfrac{\partial^2 A_2}{\partial x^2} + \dfrac{\partial^2 A_2}{\partial y^2} = -\mu_0 J \end{cases} \tag{1}$$

where the subscripts represent the areas, $A$ is the magnetic potential vector, and $J$ is the magnetic current distribution equivalent to the magnets positioned in area #2 based on Fig. 2, which can be formulated using the Fourier series as follows:

$$J = \sum_{n=1,3,\ldots}^{\infty} \alpha_n \sin(nkx), \tag{2}$$

where

$$\alpha_n = -\frac{4B_r}{\tau\mu_0}\sin\left(\frac{1}{2}nk\tau_p\right) \quad \text{and} \quad k = \pi/\tau\,.$$

In order to solve the partial differential equation system of (1), the boundary conditions are defined as follows:

$$\begin{cases} H_{1x} = 0, & y = h_m + g, \\ H_{1x} = H_{2x} \text{ and } B_{1y} = B_{2y}, & y = h_m, \\ H_{2x} = 0, & y = 0. \end{cases} \tag{3}$$

The $x$ and $y$ components of the air-gap flux density are obtained by using (4) and (5).

$$B_{1x} = -\mu_0 \sum_{n=1,3,\ldots}^{\infty} \frac{\alpha_n}{(nk)} \left( \frac{\sinh(nkh_m)}{\sinh(nk(h_m+g))} \sinh(nk(h_m+g-y)) \right) \sin(nkx), \tag{4}$$

$$B_{1y} = -\mu_0 \sum_{n=1,3,\ldots}^{\infty} \frac{\alpha_n}{(nk)} \left( \frac{\sinh(nkh_m)}{\sinh(nk(h_m+g))} \cosh(nk(h_m+g-y)) \right) \cos(nkx). \tag{5}$$

## 2.2 Slotting effects

The presence of slots in the primary leads to two basic changes in the air-gap flux density distribution: reducing its magnitude, and reshaping it. In this paper, the first and second effects are respectively applied by using Carter coefficient ($K_c$) and the relative permeance function. The effective air-gap length is calculated by using (6).

$$g_e = g + (K_c - 1) g', \tag{6}$$

where, $g'$ is the equivalent air-gap length and $g' = g + h_m/\mu_r$ . Carter coefficient is calculated as follows [13]:

$$K_c = \frac{s}{s - \gamma_1}, \tag{7}$$

$$\gamma_1 = \frac{4}{\pi} \left[ \frac{w_s}{2g} \arctan\left(\frac{w_s}{2g}\right) - \ln \sqrt{1 + \left(\frac{w_s}{2g}\right)^2} \right]. \tag{8}$$

In the next step, the slotting effects on the flux density distribution are considered by using the approach presented in [13]. It is based on the relative permeance function for a rotating permanent magnet synchronous motor. According to [13], the accurate magnetic flux density with considering slotting effects can be calculated as follows:

$$B'_g = B_g \tilde{\lambda}, \tag{9}$$

where, $B_g$ is the air-gap flux density distribution, regardless of slotting effects, $\tilde{\lambda}$ is the relative permeance function as follows:

$$\tilde{\lambda} = \alpha_0 + \sum_{j=1,2,3}^{\infty} \alpha_j \cos\left(\frac{2\pi}{s} j(x)\right), \tag{10}$$

where

$$\alpha_0 = \frac{1}{K_c}\left(1 - 1.6\beta\frac{w_s}{s}\right), \tag{11}$$

$$\alpha_j = -\beta(x)\frac{4}{\pi j}\left[\frac{1}{2} + \frac{\left(j\frac{w_s}{s}\right)^2}{0.7815 - 2\left(j\frac{w_s}{s}\right)^2}\right]\sin\left(1.6\pi j\frac{w_s}{s}\right). \tag{12}$$

It is worth to note that the complete calculation of relative permeance function can be found in [13].

## 3 Nonlinear Magnetic Equivalent Circuit

Maxwell's Equations are greatly appropriate to be applied to the intelligent machine-optimization algorithms, because of closed formulations capability for the different parameters of machine. However, it cannot model the effects of saturation. On the other hand, FEM is also not appropriate to be used in the iterative optimization algorithms, because it takes a long solution time. In order to overcome to the difficulties, the nonlinear magnetic equivalent circuit can be utilized in which the effect of core saturation is calculated via using the permeance values in the core areas based on the *B-H* curve of core material. Note that, in large scales the nonlinear magnetic equivalent circuit is equivalent to FEM. Thus, presenting a simple and accurate magnetic equivalent circuit makes it possible to be directly utilized in the iterative optimization algorithms. The permanent magnet linear synchronous motor is composed of three parts: primary, secondary, and air-gap, that magnetic equivalent circuits are all presented in following.

A limited part of primary is modeled as illustrated in Fig. 3. This part includes the magnetic permeance of teeth, the flux leakage path between the teeth, and the primary yoke. Due to the possibility of magnetic saturation, in order to model the teeth and yoke when saturation occurs, the nonlinear magnetic permeance of tooth is considered as formulated in (13)

$$P_t = \frac{h_t}{\mu_0 \mu_{re} w_t L}. \tag{13}$$

In order for regarding the ending effects in motor, the width of the ending teeth is adopted to be different from the other teeth of the motor.

The magnetic flux lines of the motor are calculated by using FEM illustrated in Fig. 4. Obviously based on the Fig. 5, it is focused view of the flux lines, some parts of the magnetic flux leaks through the path between the teeth. The permeance of the leakage path can be calculated [14] as follows;

$$P_2 = \mu_0 \frac{\pi}{4} \frac{L}{\ln\left(\frac{w_s}{s - w_s}\right)} \tag{14}$$

The slots of the motor under study are fully open, and therefore, the magnetic permeance values of two paths ($P_1$ and $P_2$) are exactly equal.

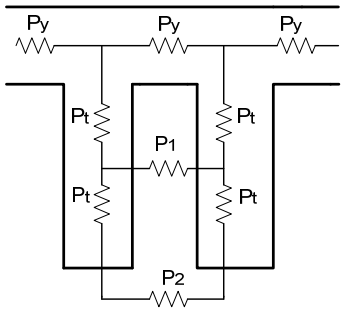


**Fig. 3** – *Modeling the slots and teeth in the proposed model.*

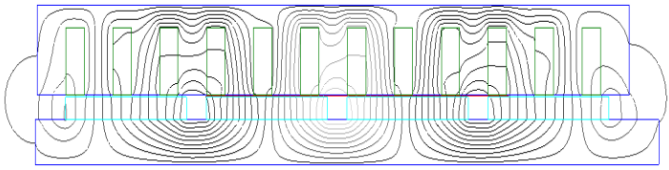

**Fig. 4** – *Distribution of the flux lines in a PM linear synchronous motor in no load operation (zero primary current).*

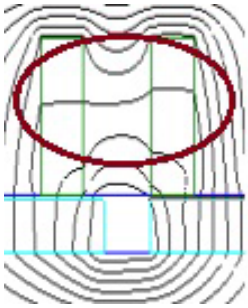

**Fig. 5** – *Focused view of flux leakage between the teeth.*

The secondary consists of the poles of permanent magnets as well as the yoke. The magnets are modeled via the equivalent flux source $F$ and the magnetic permeance $P_m$. The magnetic permeance of yoke $P_b$ is separated into two parts including, vertical and horizontal.

Modeling of air-gap is the last part of the proposed magnetic equivalent circuit. In order to extract the air-gap model, the air-gap magnetic permeance is split into two sections, the part under the slot and the tooth. Each element is connected upward to the corresponding slot or tooth, and downward to the magnet. The air-gap magnetic permeance of the area under the tooth ($P_g$), and under the slot ($P_{gs}$) are considered [14] as follows;

$$P_{gs} = \mu_0 \frac{4}{\pi} \ln\left(1 + \frac{\pi}{4}\frac{w_s}{g}\right) L\,, \tag{15a}$$

$$P_g = \mu_0 \frac{w_t L}{g}\,. \tag{15b}$$

The nonlinear magnetic equivalent circuit is finally obtained by combining the separate parts, which is shown in Fig. 6. This equivalent circuit comprises 53 elements which the magnetic permeances of yoke and tooth are both considered nonlinearly. The iterative algorithm given in [15] is used to solve this equivalent circuit, the flux and flux density. Note that, the solution of the nonlinear magnetic equivalent circuit can be achieved by using a recursive formulation that updates the values of the unknown magnetic variables in $k$ step as follows:

$$G\left(\mu_i^{(k-1)}\right) F_m^{(k)} = \Phi\left(\mu_i^{(k-1)}\right), \tag{16}$$

where $\mu_i$ is the permeability of $i^{\text{th}}$ branch, $G(\mu_i)$ is the matrix of nodal permeances, $F_m$ is the vector of nodal magnetic potentials, and $\Phi_s(\mu_i)$ represents the vector of nodal magnetic fluxes.

After solving (16), the nodal values of $\Phi(i)^{(k)}\,(i = 1,2,...,N_b)$ in $k^{\text{th}}$ step are calculated. Then, the magnetic flux density $B_m^{(k)}$ can be achieved according to the method of [15], as formulated in (17).

$$B_m^{(k)} = \Phi(i)^{(k)} / A_i\,, \tag{17}$$

where, $A_i$ denotes the cross section area of $i^{\text{th}}$ branch. Based on the magnetization curve of the magnetic material, its magnetic permeability can be obtained as follows:

$$\hat{\mu}_i^{(k)} = B_i^{(k)} / H_i^{(k)}\,, \tag{18}$$

where, $H_i^{(k)}$ is the magnetic field intensity proportional to $B_i^{(k)}$. Hence, the permeability in $k$ step is acquired according to the method presented in [15] as follows"

$$\mu_i^{(k)} = \mu_i^{(k-1)} + p_i^{(k)} \left( \hat{\mu}_i^{(k)} - \mu_i^{(k-1)} \right), \tag{19}$$

where

$$p_i^{(k)} = \min \left\{ 1.0,\ 0.01 + \frac{c_d}{\dfrac{c_d + \left| \hat{\mu}_i^{(k)} - \mu_i^{(k-1)} \right|}{\mu_i^{(k-1)}}} \right\}, \tag{20}$$

where, $p_i^{(k)}$ is the acceleration factor, $c_d$ is the descent constant which is equal to 0.6. The procedure stops when the convergence condition of (21) satisfies.

$$\left| \frac{\hat{\mu}_i^{(k)} - \mu_i^{(k-1)}}{\mu_i^{(k-1)}} \right| \le \varepsilon, \tag{21}$$

in which $\varepsilon$ is the convergence criterion whose value is adopted according to the required accuracy.

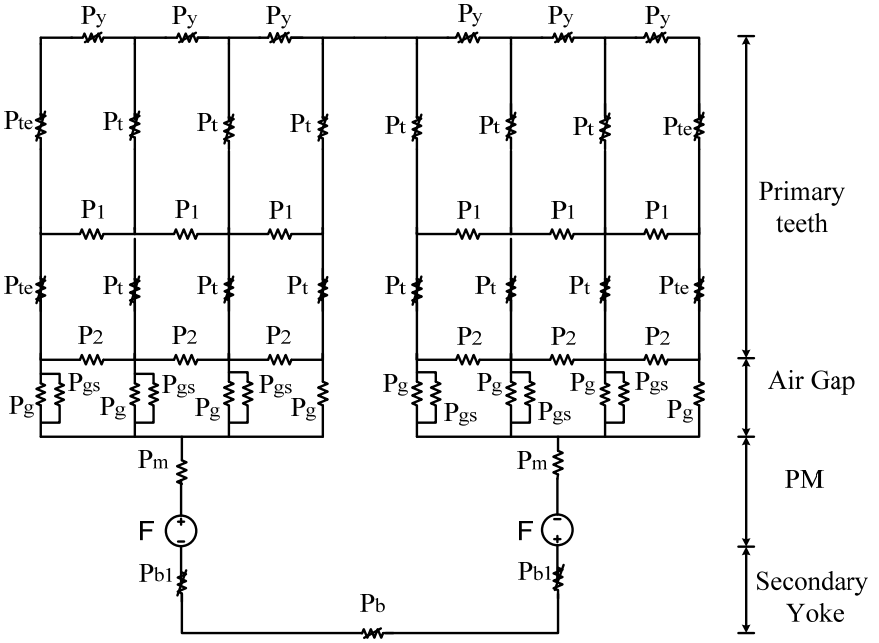


**Fig. 6** – *The nonlinear magnetic equivalent circuit associated with one pole pitch of the machine.*

## 4 Numerical Analysis

The $x$ and $y$ components of the flux density distribution in the open-circuited motor at the center of air-gap are calculated by using the Maxwell's Equations and by ignoring the slotting effects illustrated in Fig. 7. As well, the corresponding results of FEM are also depicted in those figures.

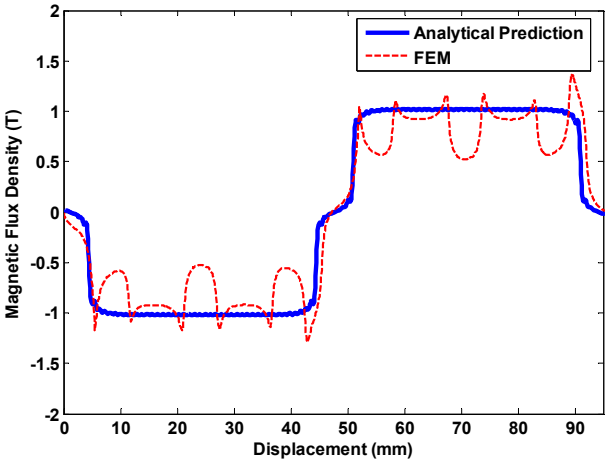


(a)

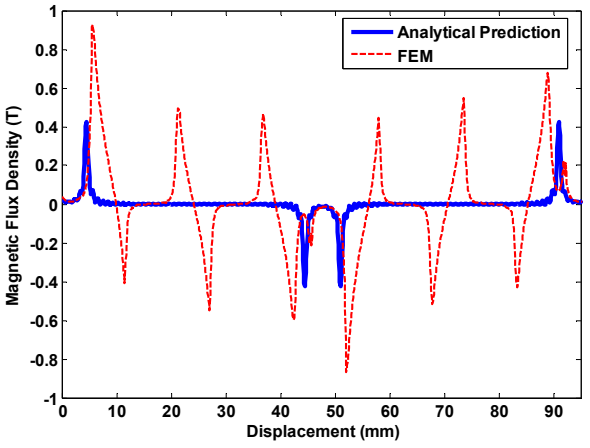


(b)

**Fig. 7** – *Comparison between the PM flux density at the center of air gap, obtained by Maxwell equations without slotting effect, and by FEM:* (a) *y component;* (b) *x component.*

It is worth to note that, the simulation results of the analytical method based on the Maxwell's Equations without considering the slotting effects are different in comparison with those obtained by the FEM. The main difference between the graphs of the two methods is related to the reduction of flux density at the areas of slots. The flux density distribution at the center of the air gap is achieved by using the relative permeance function illustrated in Fig. 8. Clearly, it can be seen that the new results using by the relative permeance function are more compatible with the FEM simulation results.

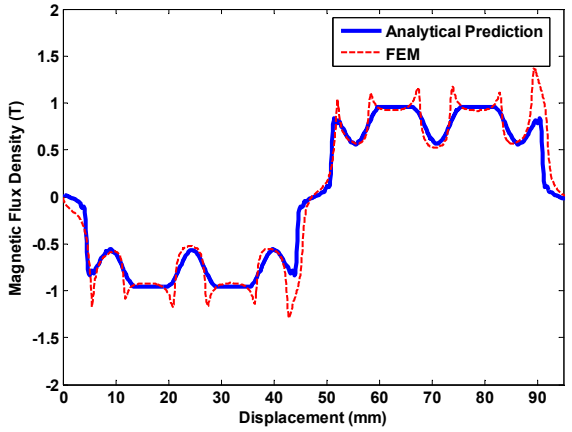


(a)

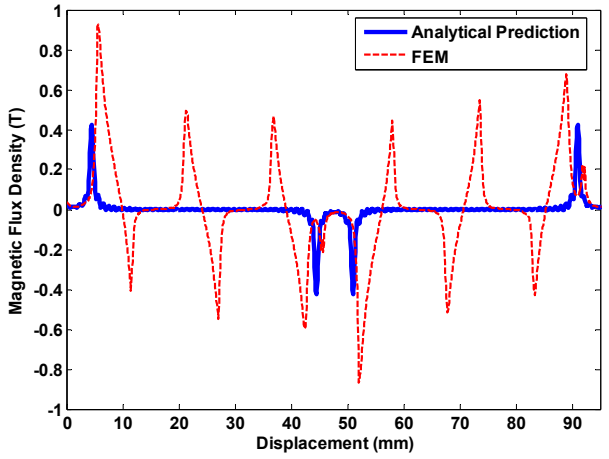


(b)

**Fig. 8** – *The same as Fig. 7, but taking into account the slotting, by means of permeance function.*

In the next step, the results achieved from nonlinear magnetic equivalent circuit are presented. Fig. 9 shows the flux density distribution of the PMLSM that is obtained by FEM. In **Table 2**, the flux density magnitudes at several positions in the motor are listed. These results are achieved by using the magnetic equivalent circuit in the both cases, with and without taking the saturation effects of iron into account. The nonlinear magnetic equivalent circuit has acceptable accuracy in comparison to FEM. The results of this table demonstrate the importance of considering the effects of core saturation in the calculation procedure of the motor parameters.

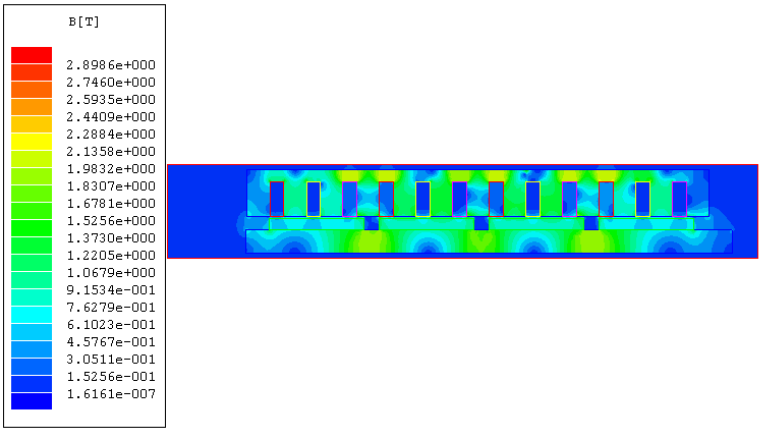


**Fig. 9** – *The flux density distribution within the PMLSM.*

**Table 2**
*Comparison among the flux density values obtained by using either of the two methods: magnetic equivalent circuit, and FEM.*

| FEM | Nonlinear model | Linear model | Position |
|---|---|---|---|
| 0.922 | 0.962 | 1.077 | At the center of air-gap |
| 1.448 | 1.4959 | 1.7468 | In the yoke of primary |
| 1.664 | 1.667 | 1.7982 | In the yoke of secondary |

The harmonic analysis of the flux density generated by the permanent magnet is performed for the three methods under study, i.e. the analytical method of solving the Maxwell's Equations with and without considering the slotting effects, the proposed model of nonlinear magnetic equivalent circuit, and FEM exhibited in the histograms of Fig. 10. The fundamental harmonic magnitude of the flux density resulted from solving the Maxwell's Equations equals to 1.01 T with considering the slotting effects, and 1.24 T when they are

disregarded. Similarly, the two methods of the nonlinear magnetic equivalent circuit and FEM also yield the values of 1.03 T and 1.04 T for the mentioned parameter, respectively. Moreover, the nonlinear magnetic equivalent circuit gives better results for calculating the harmonic orders of the flux density in the comparison with Maxwell's Equations.

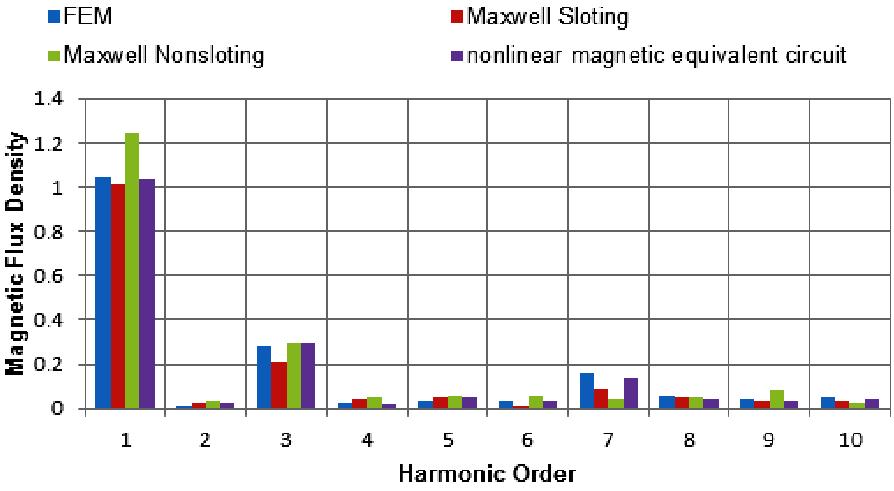


**Fig. 10** – *Harmonic analysis of the flux density waveform created by the permanent magnet.*

## 5 Conclusion

In this paper, an accurate analytical model to calculate the flux density waveform and its harmonics is presented that it can easily be used in the iterative optimization algorithms (e.g. Genetic Algorithm). First, the magnetic analysis of the permanent magnet linear synchronous motor has been performed by using three methods, including Maxwell's Equations, nonlinear magnetic equivalent circuit, and FEM. Although the method of Maxwell's equations introduces some closed formulations for the motor parameters, it cannot consider the effect of core saturation. On the other hand, the FEM is not appropriate for being used in the intelligent machine-optimization algorithms, because it usually takes long solution time. To overcome the difficulties, this paper has presented a nonlinear magnetic equivalent circuit which can be applied to the iterative optimization algorithms, due to an accuracy and less solution time. The comparison between the numerical results of the proposed model against the FEM obviously demonstrates the validity of the nonlinear magnetic equivalent circuit.

# 6 Appendix A

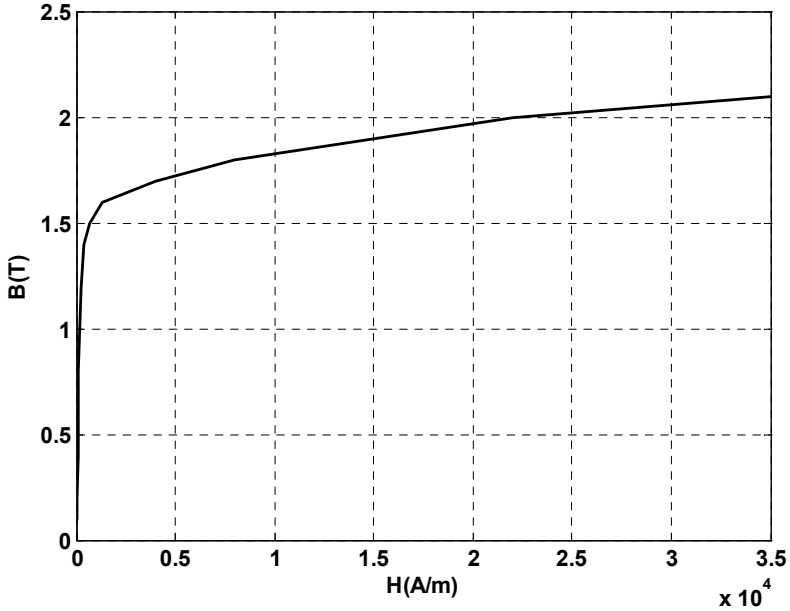


**Fig. A1** – *Magnetizing curve B-H of* DK66 [1].

# 6 References

[1] J.F. Gieras, Z.J. Piech: Linear Synchronous Motors: Transportation and Automation Systems, CRC Press, Boca Raton, FL, USA, 2000.

[2] I. Boldea, S.A. Nasar: Linear Motion Electromagnetic Devices, Taylor and Francis, NY, USA, 2001.

[3] G.H. Kang, J.P. Hong, G.T. Kim: A Novel Design of an Air-Core Type Permanent Magnet Brushless Motor by Space Harmonic Field Analysis, IEEE Transaction on Magnetics, Vol. 37, No. 5, Sept. 2001, pp. 3732 – 3736.

[4] G.H. Kang, J.P. Hong, G.T. Kim: Design and Analysis of Slotless Type Permanent Magnet Linear Brushless Motor by using Equivalent Magnetizing Current, IEEE Transaction on Industry Application, Vol. 37, No. 5, Sept/Oct. 2001, pp. 1241 – 1247.

[5] K.C. Lim, J.K. Woo, G.H. Kang, J.P. Hong, G.T. Kim: Detent Force Minimization Techniques in Permanent Linear Synchronous Motors, IEEE Transaction on Magnetics, Vol. 38, No. 2, March 2002, pp. 1157 – 1160.

[6] M. Inoue, H. Sato: An Approach to a Suitable Stator Length for Minimization the Detent Force of Permanent Magnet Linear Synchronous Motors, IEEE Transaction on Magnetics, Vol. 36, No. 4, July 2000, pp. 1890 – 1893.

[7] D.Y. Lee, G.T. Kim: Design of Thrust Ripple Minimization by Equivalent Magnetizing Current Considering Slot Effect, IEEE Transaction on Magnetics, Vol. 42, No. 4, April 2006, pp. 1367 – 1370.

[8] N. Chayopitak, D.G. Taylor: Performance Assessment of Air-Core Linear Permanent-Magnet Synchronous Motors, IEEE Transaction on Magnetics, Vol. 44, No. 10, Oct. 2008, pp. 2310 – 2316.

[9] I.S. Jung, J. Hur, D.S. Hyun: 3-D Analysis of Permanent Magnet Linear Synchronous Motor with Magnet Arrangement using Equivalent Magnetic Circuit Network Method, IEEE Transaction on Magnetics, Vol. 35, No. 5, Sept. 1999, pp. 3736 – 3738.

[10] S. Vaez-Zadeh, A.H. Isfahani: Enhanced Modeling of Linear Permanent Magnet Synchronous Motors, IEEE Transaction on Magnetics, Vol. 43, No. 1, Jan. 2007, pp. 33 – 39.

[11] S.G. Lee, S.A. Kim, S. Saha, Y.W. Zhu, Y.H. Cho: Optimal Structure Design for Minimizing Detent Force of PMLSM for a Ropeless Elevator, IEEE Transaction on Magnetics, Vol. 50, No. 1, Jan. 2014, p. 4001104.

[12] N.R. Tavana, A. Shoulaie, V. Dinavahi: Analytical Modeling and Design Optimization of Linear Synchronous Motor with Stair-Step-Shaped Magnetic Poles for Electromagnetic Launch Applications, IEEE Transaction on Plasma Science, Vol. 40, No. 2, Feb. 2012, pp. 519 – 527.

[13] Z.Q. Zhu, D. Howe: Instantaneous Magnetic Field Distribution in Brushless Permanent Magnet DC Motor - Part III: Effect Of Stator Slotting, IEEE Transaction on Magnetics, Vol. 29, No. 1, Jan. 1993, pp. 143 – 151.

[14] K. Akatsu, S. Wakui: A Comparison Between Axial and Radial Flux PM Motor by Optimum Design Method from the Required Output NT Characteristics, COMPEL – The International Journal for Computation and Mathematics in Electrical and Electronic Engineering, Vol. 25, No. 2, March 2006, pp. 496 – 509.

[15] M. Cheng, K.T. Chau, C.C. Chan, E. Zhou, X. Huang: Nonlinear Varying-Network Magnetic Circuit Analysis for Doubly Salient Permanent Magnet Motors, IEEE Transaction on Magnetics, Vol. 36, No. 1, Jan. 2000, pp. 339 – 348.